NAVAL POSTGRADUATE SCHOOL

MONTEREY, CALIFORNIA

THESIS

EFFECTS OF LABORATORY ROLLING CONDITIONS ON CONTINUOUSLY CAST AA5083

by

Matthew F. Thompson

June 2007

Thesis Advisor:	Terry McNelley
Co-advisor:	Srinivasan Swaminathan

Approved for public release; distribution is unlimited

THIS PAGE INTENTIONALLY LEFT BLANK

REPORT DOCUMENTATION PAGE		Form Approved OMB No. 0704-0188

1. AGENCY USE ONLY *(Leave blank)*	2. REPORT DATE	3. REPORT TYPE AND DATES COVERED
	June 2007	Master's Thesis

4. TITLE AND SUBTITLE Effects of Laboratory Rolling Conditions on Continuously Cast AA5083	5. FUNDING NUMBERS
6. AUTHOR(S) Matthew Thompson	
7. PERFORMING ORGANIZATION NAME(S) AND ADDRESS(ES) Naval Postgraduate School Monterey, CA 93943-5000	8. PERFORMING ORGANIZATION REPORT NUMBER
9. SPONSORING /MONITORING AGENCY NAME(S) AND ADDRESS(ES) N/A	10. SPONSORING/MONITORING AGENCY REPORT NUMBER

11. SUPPLEMENTARY NOTES The views expressed in this thesis are those of the author and do not reflect the official policy or position of the Department of Defense or the U.S. Government.

12a. DISTRIBUTION / AVAILABILITY STATEMENT	12b. DISTRIBUTION CODE
Approved for public release; distribution is unlimited	

13. ABSTRACT (maximum 200 words)

Quick Plastic Forming (QPF) is a recent adaptation of Superplastic Forming (SPF) that allows economical fabrication of complex components using superplastic material. QPF requires refined, equiaxed grains and high-angle grain boundaries in the microstructure to enhance sheet deformation by GBS at the high strain rates involved. This study evaluates the effects of laboratory rolling conditions on continuously cast AA5083 in the hot-band condition in anticipation of QPF. Orientation imaging microscopy, scanning electron microscopy and X-ray analysis were used to analyze roles of the geometric dynamic recrystallization and particle stimulated nucleation of recrystallization in the microstructure evolution during rolling. A refined microstructure was developed during the rolling procedures but mechanical property data indicated low to moderate ductility and failure by excessive cavity formation. Factors influencing the development of microstructure and mechanical properties during laboratory rolling were investigated.

14. SUBJECT TERMS Superplasticity, Superplastic deformation, Quick plastic deformation, AA 5083, Warm rolling, Roll gap geometry, Rolling conditions	15. NUMBER OF PAGES 59
	16. PRICE CODE

17. SECURITY CLASSIFICATION OF REPORT	18. SECURITY CLASSIFICATION OF THIS PAGE	19. SECURITY CLASSIFICATION OF ABSTRACT	20. LIMITATION OF ABSTRACT
Unclassified	Unclassified	Unclassified	UL

NSN 7540-01-280-5500 Standard Form 298 (Rev. 2-89)
Prescribed by ANSI Std. 239-18

THIS PAGE INTENTIONALLY LEFT BLANK

Approved for public release; distribution is unlimited

EFFECTS OF LABORATORY ROLLING CONDITIONS ON CONTINUOUSLY CAST AA5083

Matthew F. Thompson
Lieutenant, United States Navy
B.S., United States Naval Academy, 2000

Submitted in partial fulfillment of the
requirements for the degree of

MASTER OF SCIENCE IN MECHANICAL ENGINEERING

from the

NAVAL POSTGRADUATE SCHOOL
June 2007

Author: Matthew Thompson

Approved by: Terry McNelley
Thesis Advisor

Srinivasan Swaminathan
Co-advisor

Anthony J. Healey
Chairman, Department of Mechanical and Astronautical Engineering

THIS PAGE INTENTIONALLY LEFT BLANK

ABSTRACT

Quick Plastic Forming (QPF) is a recent adaptation of Superplastic Forming (SPF) that allows economical fabrication of complex components using superplastic material. QPF requires refined, equiaxed grains and high-angle grain boundaries in the microstructure to enhance sheet deformation by GBS at the high strain rates involved. This study evaluates the effects of laboratory rolling conditions on continuously cast AA5083 in the hot-band condition in anticipation of QPF. Orientation imaging microscopy, scanning electron microscopy and X-ray analysis were used to analyze roles of the geometric dynamic recrystallization and particle stimulated nucleation of recrystallization in the microstructure evolution during rolling. A refined microstructure was developed during the rolling procedures but mechanical property data indicated low to moderate ductility and failure by excessive cavity formation. Factors influencing the development of microstructure and mechanical properties during laboratory rolling were investigated.

THIS PAGE INTENTIONALLY LEFT BLANK

TABLE OF CONTENTS

THIS PAGE INTENTIONALLY LEFT BLANK

LIST OF FIGURES

LIST OF TABLES

THIS PAGE INTENTIONALLY LEFT BLANK

ACKNOWLEDGMENTS

The author would like to extend his immense gratitude to Professor Terry McNelley for his profound guidance in this research. The author also wishes to thank Dr. Srinivasan Swaminathan for his tireless effort and assistance during the microscopy portion of the study.

Finally, the author would like to extend his appreciation to his loving and supporting wife who has endured the long hours put into this project. Tell Sydney and Mason that daddy is coming home!

THIS PAGE INTENTIONALLY LEFT BLANK

EXECUTIVE SUMMARY

Quick Plastic Forming (QPF) is a recent adaptation of Superplastic Forming (SPF) that allows economical fabrication of complex components using superplastic material. QPF requires refined, equiaxed grains and high-angle grain boundaries in the microstructure to enhance sheet deformation by GBS at the high strain rates involved. This study evaluates the effects of laboratory rolling conditions on continuously cast AA5083 in the hot-band condition in anticipation of QPF. Orientation imaging microscopy, scanning electron microscopy and X-ray analysis were used to analyze roles of the geometric dynamic recrystallization and particle stimulated nucleation of recrystallization in the microstructure evolution during rolling. A refined microstructure was developed during the rolling procedures but mechanical property data indicated low to moderate ductility and failure by excessive cavity formation. Factors influencing the development of microstructure and mechanical properties during laboratory rolling were investigated.

THIS PAGE INTENTIONALLY LEFT BLANK

I. INTRODUCTION

Among the major considerations in the United States' naval shipbuilding program has been the most effective and cost efficient materials and manufacturing methods. These methods, coupled with keeping production time low and obtaining products of the highest quality, have kept the navy interested in aluminum alloys since World War II. It was during the war that developments in arc welding allowed it to become a legitimate alternative to riveting as the joining technique for aluminum. The 5xxx-series aluminum alloys (Al-Mg system) are widely used in many manufacturing applications because they are relatively inexpensive while possessing attractive engineering properties, such as: moderate strength, acceptable weldability, corrosion resistance and ease of surface treatment. [2, 3] Another advantage of aluminum is its strength / weight ratio in comparison to steel. AA5083 is widely used for structural and other maritime applications. One of the U.S. Navy's newest warships, the Littoral Combat Ship (LCS), is currently under construction and is designed to have an aluminum superstructure.

A drawback in using aluminum during the manufacturing process is its lack of formability when compared to steel. Aluminum alloys that can be easily formed usually lack sufficient strength. Aluminum alloys of sufficient strength cannot be formed into complex shapes and, instead, they must be fabricated using methods such as hot forging or extrusion.

An alternative way of forming involves superplastic forming (SPF) that is typically achieved by subjecting a heated sheet of superplastic material to a pressure differential in a chamber to form complex shapes as illustrated in Figure 1.

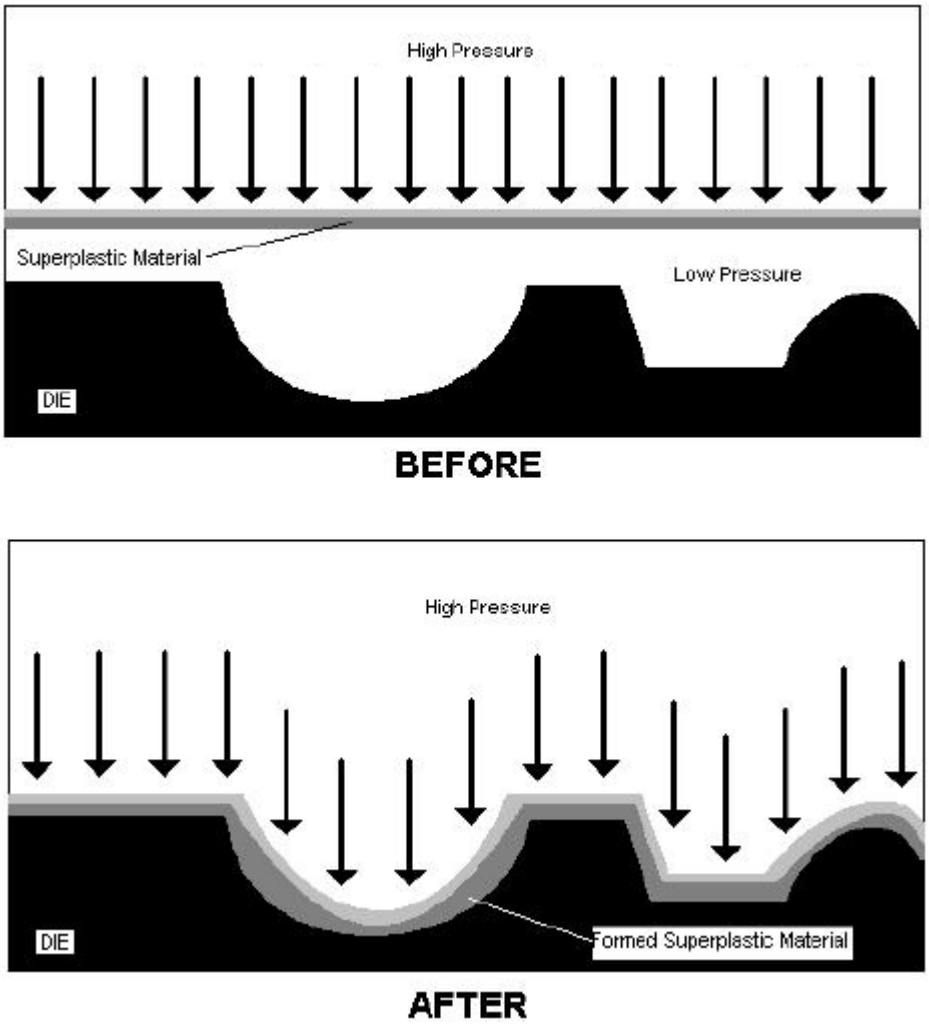

Figure 1. Schematic of superplastic forming process. [1]

To attain complex shapes, SPF material must exhibit large tensile elongations. In comparison to forming steel parts where two dies are required for stamping and a high work input is needed, SPF requires only one die. Forces are not high and SPF therefore demands a much lower work input. However, SPF requires low strain rates and high temperatures for the grain boundary sliding (GBS) mechanism that results in its high elongations. These low strain rates slow production times and this loss in product volume usually offsets the gain of lower work input achieved by the SPF process. A recently

researched variant of SPF is Quick Plastic Forming (QPF), a process that is similar to SPF but may be accomplished at higher strain rates.

Quick plastic forming is faster than SPF, subjecting the superplastic material to higher strain rates. Development of the QPF process within General Motors is based on an integrated reengineering of all SPF technology elements that do not fit the high-volume needs of mainstream automotive products. QPF has now reached a state of maturity where it can compete with other limited volume manufacturing systems and with further developments could enable even higher volume production. Thus far, QPF has been employed with Al-Mg alloys and takes advantage of solute drag creep (SDC) which facilitates high ductility under QPF conditions [4].

It has been documented that a higher level of superplasticity may be obtained through specific processing methods. Warm rolling is thought to have a beneficial affect by refining grain size and controlling texture. The aim of this research was to evaluate the effects of cold and warm rolling AA5083 material in a laboratory setting in anticipation of a QPF process.

THIS PAGE INTENTIONALLY LEFT BLANK

II. BACKGROUND

A. SUPLASTICITY

Superplasticity is "the ability of a polycrystalline material to exhibit, in a generally isotropic manner, very high tensile elongations prior to failure" [4].
Superplastic materials exhibit large values of the strain-rate sensitivity coefficient, *m*, during deformation. The flow stress strain-rate is expressed as

$$\sigma = \frac{F}{A} = K\dot{\varepsilon}^{m} \quad [7]\ \text{Eq.1}$$

where σ is flow stress, F is applied force, A is cross-sectional area, K is a material constant, and $\dot{\varepsilon}$ is the true strain rate [7]. Values of $m > 0.33$ are typical in superplastic materials. Ordinary metals and alloys exhibit values of $m \approx 0.2$ and, for materials such as hot glass, *m* approaches unity during tensile deformation. A high value of *m* usually indicates sufficient resistance to necking which allows superplastic flow to be possible. It is commonly accepted that fine-structure superplasticity (FSS) primarily relies on Grain Boundary Sliding (GBS) as the deformation mechanism. The GBS must be accompanied by an accommodating mechanism to ensure grain rearrangement during deformation [10]. The accommodating mechanism is believed to be the rate-controlling process and restricts superplasticity to relatively low strain rates (10^{-4}/s to 10^{-3}/s). Figure 2 displays the typical sigmoidal shape of the flow stress verses strain rate on a double logarithmic scale. Region I deformation mechanisms are not well understood. Region II is predominantly controlled by GBS and in Region III Dislocation Slip (DS) becomes the primary deformation mechanism.

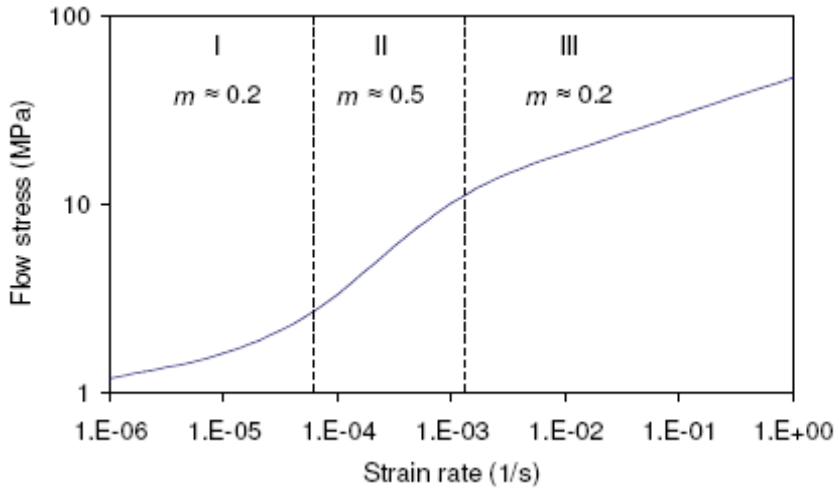

Figure 2. Typical sigmoidal strain-rate dependence of the flow stress for a conventional fine-grained superplastic material.

When GBS is the prominent deformation mechanism, strain rates increase as grain size decreases. Therefore, FSS requires a material with a stable, refined grain structure of usually less than 10μm. In addition to fine grain size, FSS in metal based materials requires equiaxed grains, high angle boundaries (>15°) and the presence of second phase particles.

The DS processes typically involve dislocation glide and climb within grains and are not grain-size dependant. Solute additions in Al, such as Mg, often lead to SDC wherein dislocation glide becomes rate controlling. This results in increased m values of up to 0.3 in Region III and this is thought to enhance ductility during deformation at strain rates in the vicinity of the transition from Region II to Region III.

Due to the severe limitations on manufacturing volumes caused by the slow strain rates of traditional SPF, General Motors began research into QPF. Despite improvements in the process, there is still research to be done before QPF can be used on a large manufacturing level.

B. QUICK PLASTIC FORMING

Quick plastic forming is conducted under strain rates where both GBS and SDC contribute to the deformation process. Similar to SPF, since GBS is enhanced by grain refinement while SDC is independent of grain size, QPF is also enhanced by grain refinement. [18]. Grain size refinement enhances ductility because the value of *m* is greater for GBS than for SDC and grain refinement thereby increases the strain rate range for GBS to contribute to deformation that enhances QPF response.

Currently AA5083 materials for QPF are produced by the direct chill (DC) method. Direct chill casting involves the production of ingots that are typically 300 mm in thickness. Such ingots are hot and warm rolled to a hot band (HB) condition that is typically between 4-6 mm in thickness. Recent interest has developed in continuously cast (CC) materials; continuous castings are typically 15 mm in thickness in the as-cast condition. The use of CC material may lead to cost savings and this has led to this investigation. It is anticipated, due to the nature of the CC process verses the DC process, that the CC material will exhibit an inhomogeneous microstructure in the HB condition due to less strain being imparted and this will likely be reflected in the final rolled microstructure.

Geometric dynamic recrystallization (GDRX) is a process in which a refined and nearly equiaxed grain structure is formed, because grain boundaries which have become serrated during formation of subgrains in the course of hot deformation recombine as serrations pinch off or as the grains thin down. At lower deformation temperatures grain boundaries do not interact as readily with the substructure and grains continue to elongate without serration [11]. It is believed that the process of GDRX may be induced under warm rolling conditions and create a very fine grain structure. The roll of GDRX during warm and cold rolling will be examined.

THIS PAGE INTENTIONALLY LEFT BLANK

III. EXPERIMENTAL PROCEDURES

A. OVERVIEW

In this investigation, AA5083 aluminum-magnesium alloys that had been processed for grain refinement and superplasticity were examined. Specifically, continuously cast AA5083, in the hot-band condition and designated G1 which had been provided by the General Motors Corporation, as examined.

The program for investigation comprised three major steps. First, the as-received G1 material was analyzed for microstructure and texture. Next, the as-received HB G1 material was rolled to 74% reduction under two temperature conditions; room temperature (RT) and 300°C. The rolled material was analyzed for microstructure and texture. Finally, the as-rolled material was tensile tested at various strain rates at 450°C, to determine mechanical properties. All analysis was done using optical microscopy (OM), scanning electron microscopy (SEM), orientation imaging microscopy (OIM) and X-ray.

B. MATERIALS

Samples of the AA5083, G1 material, were provided in the form of as-rolled sheet material. The 5083 material composition (in wt. pct.) is provided in Table 1.

Element	Si	Fe	Cu	Mn	Mg	Cr	Zr	Al
Wt % for G1	0.102	0.191	0.025	0.735	4.616	0.249	0.001	Bal

Table 1. Chemical composition data for AA5083, G1 material.

The material was supplied by General Motors in the as-cast (AC) condition with an initial thickness of 15 mm, and the HB condition, with a thickness of 4 mm.

As-received HB samples were rolled to 74% reduction at RT and 300°C using the schedule in Table 2. The resulting true strains are presented in Table 3.

Passes	Reduction (%)	Anticipated Rebound (%)
1	25	20
2	20	20
3	20	10
4	20	0
5	20	0
6	15	0

Table 2. Rolling schedule for 74% reduction of HB AA5083, G1 material.

Processing by General Motors	True Strain
	1.32

(a)

Number of passes	True Strain-RT	True Strain-300°C	Cumulative Strain-RT	Cumulative Strain-300°C
1	0.239	0.136	1.55	1.46
2	0.280	0.246	1.84	1.70
3	0.298	0.239	2.17	1.94
4	0.225	0.235	2.36	2.18
5	0.225	0.231	2.59	2.41
6	0.199	0.223	2.79	2.63

(b)

Table 3. Cumulative and per pass true strains induced during processing AA5083, G1, material from, (a) AC to HB condition (b) HB condition to 74% reduction.

Samples were rolled to a final thickness of 0.91 mm and 1.02 mm, at RT and 300°C, respectively.

C. SAMPLE PREPARATION

1. Optical and Scanning Microscopy and X-ray

Sample preparation for optical microscopy began with mounting the samples in Red Phenolic Premolds by using a Buehler Simpliment 2 mounting press. All samples for optical and scanning electron microscopy, and X-ray analysis underwent a grinding/polishing procedure as outlined in Table 4. The samples were subjected to successively finer silicon carbide abrasives for initial grinding. The grinding was done on a Buehler Ecomet 4 rotating wheel and with continuous lubrication by water. Minimal downward pressure was applied and maintained until evidence of the prior grinding step was removed. Between steps the sample was flushed with water to remove any residual sediment. Polishing was done using a fastened polishing cloth on a Buehler Ecomet 3 rotating wheel. Polishing solutions were dilute, water-based diamond suspensions although the last step was a colloidal silica. After each grinding/polishing step, ultrasonic cleaning was conducted for 5 minutes with methanol.

Step	Abrasive	Time	RPM
1	320 Grit SiC Paper	5 min	30
2	1000 Grit SiC Paper	5 min	30
3	2400 Grit SiC Paper	5 min	30
4	4000 Grit SiC Paper	5 min	30
5	1 µm Metadi Diamond Suspension	15 min (2.5 min/axis)	160
6	3 µm Metadi Diamond Suspension	15 min (2.5 min/axis)	160
7	.05 µm Colloidal Silica	15 min (2.5 min/axis)	90

Table 4. Mechanical Grinding/Polishing Procedure

2. Orientation Imaging Microscopy

Sample preparation for OIM was conducted as outlined in Table 4 with an additional electro-polishing step. An electropolishing was conducted to achieve a distortion-free surface and maximize the diffraction pattern quality. This final polishing

was conducted with a Buehler Electromet 4 Electropolisher set to a voltage needed to achieve a current density of 1.5 A/cm^2 for 20 sec. The electrolyte solution used was 75% Methanol and 25% Nitric Acid. The samples were rinsed in Methanol and either directly placed in the SEM for analysis or stored in Methanol to prevent oxidation before examination.

3. Tensile Samples

Samples for tensile testing were cut using a Charmilles Andrew Traveling Wire Electrical Discharge Machine (EDM) System. The EDM is best described as electronic spark erosion. The tensile samples were cut from the center of the rolled materials with the axis of the samples parallel to the rolling direction. The geometry of the tensile sample is described in Figure 3. Once cut, the samples were lightly sanded on all sides with 320 Grit SiC paper to remove any superficial defects. The samples were equilibrated at 450°C for 50 min immediately prior to tensile testing.

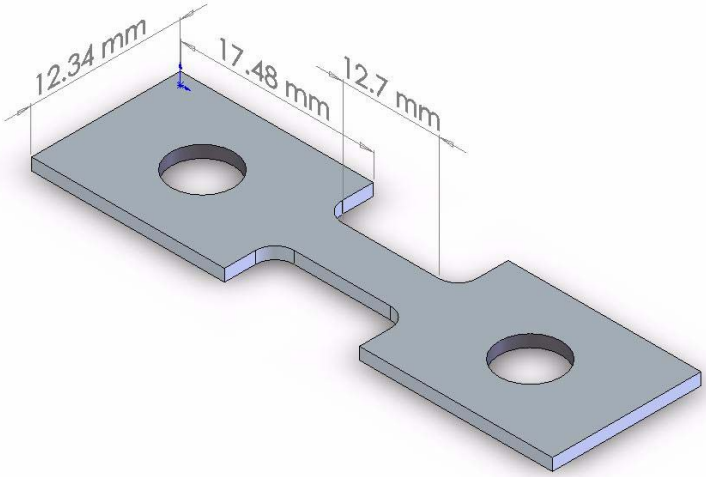

Figure 3. Schematic of tensile sample used in strain deformation tests

D. EQUIPMENT PROCEDURES

1. Optical

Optical microscopy was conducted using a Nikon Model Epiphot 200 inverted metallograph. Optical microscopy images were taken using a Digital Sight Ds-2Mv camera and pictures were collected using iSolutions Lite software. The fractography pictures were acquired on the RD-TD plane. Microstructure was analyzed on the RD-ND plane, as illustrated in Figure 4.

2. Scanning Electron and Orientation Imaging Microscopy

In orientation imaging microscopy (OIM) on aluminum alloys, extreme care must be taken to ensure a smooth, uniform surface because the region from which the electron backscatter diffraction are formed extends only to a depth of 50 nm below the surface [8]. The OIM was conducted on a TOPCON S-510 SEM operating at 15 kV with a LaB6 filament and a step-size used was either 0.1 or 0.3μm. The OIM study involved standard clean-up procedures [19]: (i) grain dilatation with a grain tolerance angle (GTA) of 5°; a minimum grain size (MGS) of two pixels; (ii) grain confidence index (CI) standardization with GTA=5° and MGS=2; and (iii) neighbor CI correlation with minimum CI of 0.1. OIM was conducted on the RD-ND plane, as illustrated in Figure 3.2, on the as received HB material after annealing for one hour at 300°C and the rolled to 74% reduction material at RT and 300°C conditions.

SEM fractography was conducted on the TD-ND plane, after tensile testing, at the fracture.

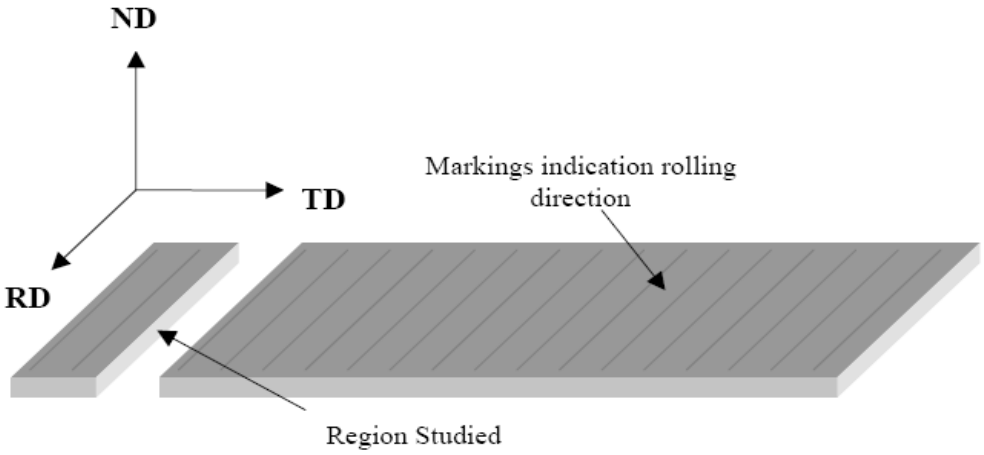

Figure 4. Schematic of sample in as-rolled condition. RD, ND, TD labels on the axis represent rolling, normal, and transverse directions respectively. The samples were sectioned along RD to examine microstructure induced by rolling.

3. X-ray

X-ray analysis was conducted with a Philips Analytical X-Ray PW 1830 diffractometer. Samples were analyzed at 30 kV and 35 mA. Samples were scanned using X'Pert Data Collector software by initially measuring intensity levels at the approximate 2θ angles, as illustrated in Figure 5, that correlate to the highest intensities expected for aluminum alloys according to Bragg's Law [9]. Scans were administered by analyzing 0.5 degrees below and above the expected angle of highest intensity with a step size of 0.040° and a time of 2.0 seconds per step for a scan speed of 0.020 °/s. The 2θ angles of highest X-ray intensities were 38.285°, 44.515°, 64.775° and 77.820° for the 111, 200, 220 and 311, lattice planes, respectively. These 2θ angles were used to conduct comprehensive examinations of the samples using continuous scan mode for Φ angle ranges between 0° to 360° at a step size of 5° and a time of 1 second per step for a scan speed of 5 °/s. After each 360° scan of the Φ angle was completed the χ angle was adjusted 5 degrees. This was continued for the χ angle range between 0° and 85°. The Φ and χ angles are illustrated in Figure 5.

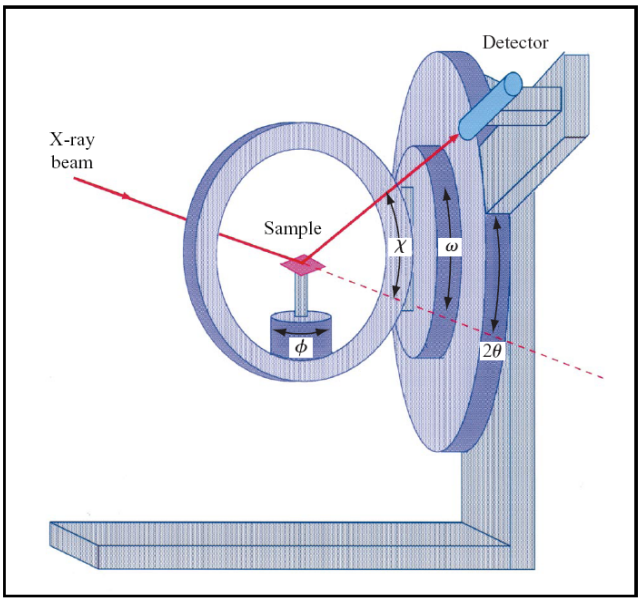

Figure 5. Schematic showing the 2θ, Φ and χ angles in relation to the incident X-ray beam, the sample and the diffracted X-ray beam.

4. Rolling

Warm rolling was accomplished by heating the material to 300°C in a furnace within immediate vicinity of the rolling mill. Initial heating was done for one hour. After each subsequent pass, heating was done for 10 minutes. Transfer of material from furnace to rolling mill took approximately 3 seconds.

5. Tensile Testing

Tensile testing was conducted using an Instron 4507 Universal Solids Testing Machine with a 10 kN load cell. The samples were tested at six constant strain rates between 1 x 10^{-4} and 3 x 10^{-2}/s. The samples were tested at 450°C. Results were calculated using Series IX Instron software. Crosshead speed of the Instron machine was determined using the equation

$$\dot{\varepsilon} = \frac{V}{l * 60} /\text{s} \quad \text{Eq. 2}$$

where $\dot{\varepsilon}$ is the strain rate, V is the crosshead speed in mm/min and l is the gauge length of the tensile sample. Tests were conducted at a constant crosshead speed. The data file from the Instron includes the elastic deflection of the load cell and linkages to the sample. A MATLAB program was written to enable the reduction of the data to true stress versus true plastic strain.

IV. RESULTS

A. AS-RECEIVED AA5083 G1 MATERIAL

Optical microscopy (OM) of the as-received material showing elongated grains representative of rolling as seen in Figure 6. Numerous OM images were analyzed to determine an approximate grain size between 20 and 120μm as seen in Figure 7.

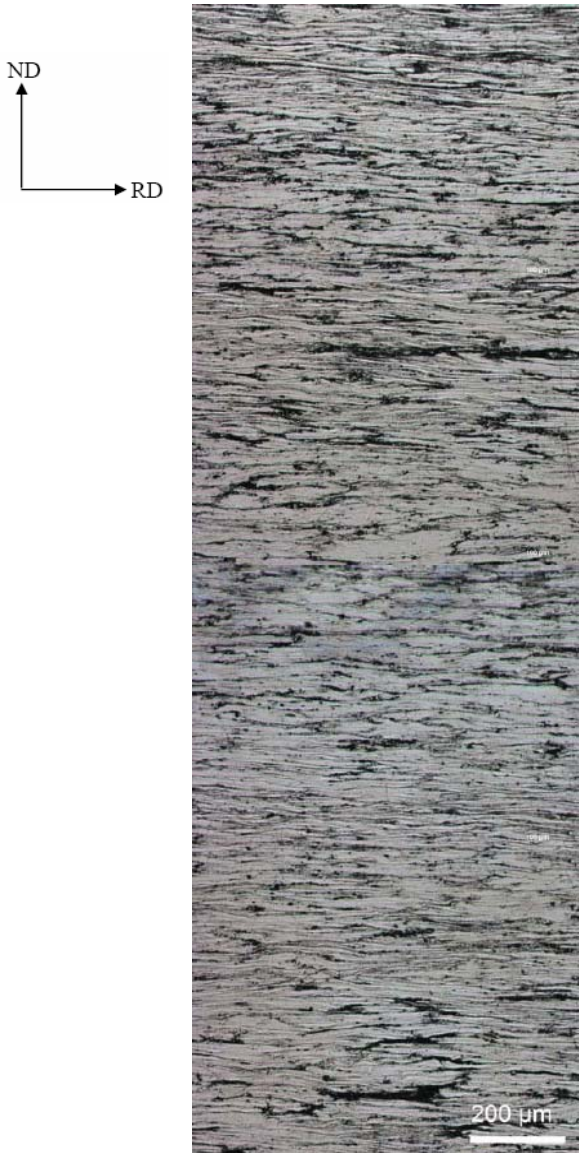

Figure 6. Optical microscopy of cross-section of received HB AA5083 showing elongated grains in the rolling direction.

Figure 7. Optical microscopy of received HB AA5083 showing elongated grains having widths between 20 -120 µm.

OIM analysis for the as-received HB material was conducted to determine microstructure and microtexture for comparison to subsequent rolling of the material. A unique grain color image and a corresponding grayscale image, reflecting image quality, of the received G1, HB material after being annealed for one hour at 300°C is shown in Figure 8. The images reveal a mixture of larger highly elongated grains and finer grains corresponding to a deformed rolling texture assumed to be the result of processing by from the as-cast to the HB condition. The darker regions in the grayscale image resulting in lower image quality may originate from regions of high dislocation density resulting from high strain in the material induced by processing. Rotated pole figure (in RD-TD direction) data pictured in Figure 8 also represents the presence of elongated grains related to the rolling. The rolling texture is predominantly a deformation texture with mainly β-fiber orientations and it is apparent the material has not recrystallized.

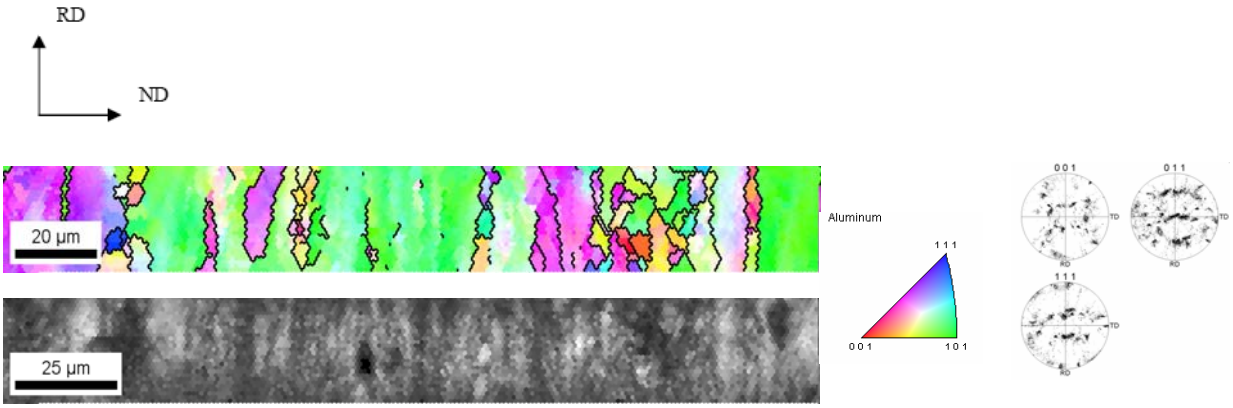

Figure 8. IPF map, IQ map along the RD-ND direction and rotated pole figure (in RD-TD direction) of HB material annealed at 300°C for 1 hour showing the presence of elongated grains having rolling texture.

X-ray analysis of the as-received G1, HB material shows the presence of a rolling texture in both the original HB and HB annealed for one hour at 300°C conditions. The rolling texture shown in Figure 9 validates the OIM data of possessing a β-fiber rolling texture.

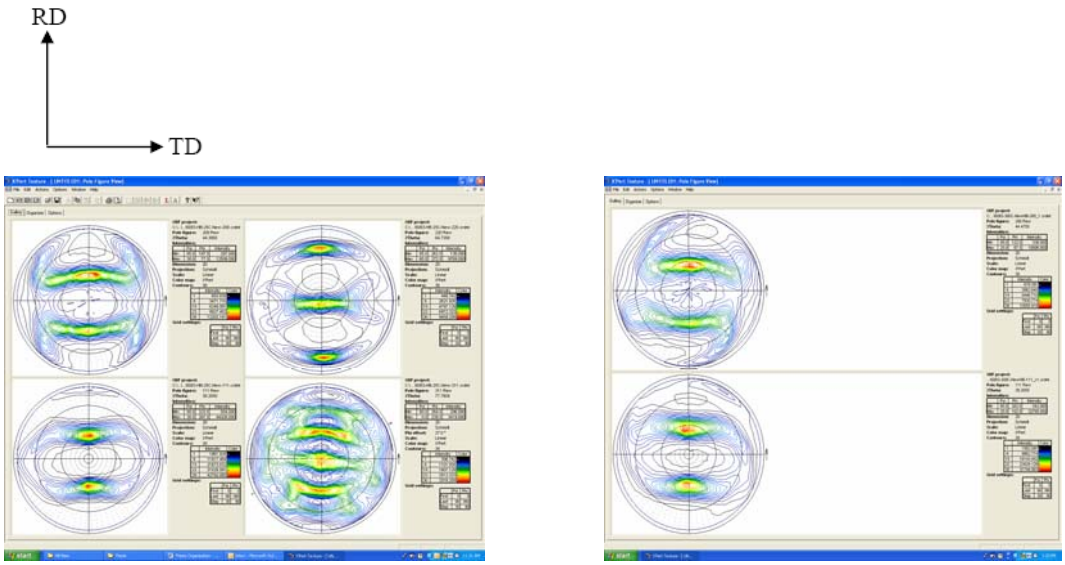

(a) (b)

Figure 9. X-ray pole figures from RD-TD plane of (a) as-received HB and (b) as-received HB annealed at 300°C for one hour. Both show the presence of rolling texture.

B. ROLLED AA5083 G1 MATERIAL

Unique grain color images and corresponding grayscale images for the G1 material rolled to 74% reduction at RT and 300°C are displayed in Figure 10 and Figure 11, respectively. Towards the center of both samples a mixture of larger, highly elongated grains and finer grains are shown that correspond to a deformation rolling texture as seen in the HB prior to rolling condition. Closer to the surface of the material, however, the microstructure appears to consist of randomly oriented, equiaxed grains that may correspond to a shear texture, or C component, induced by the geometry of the rolling mill.

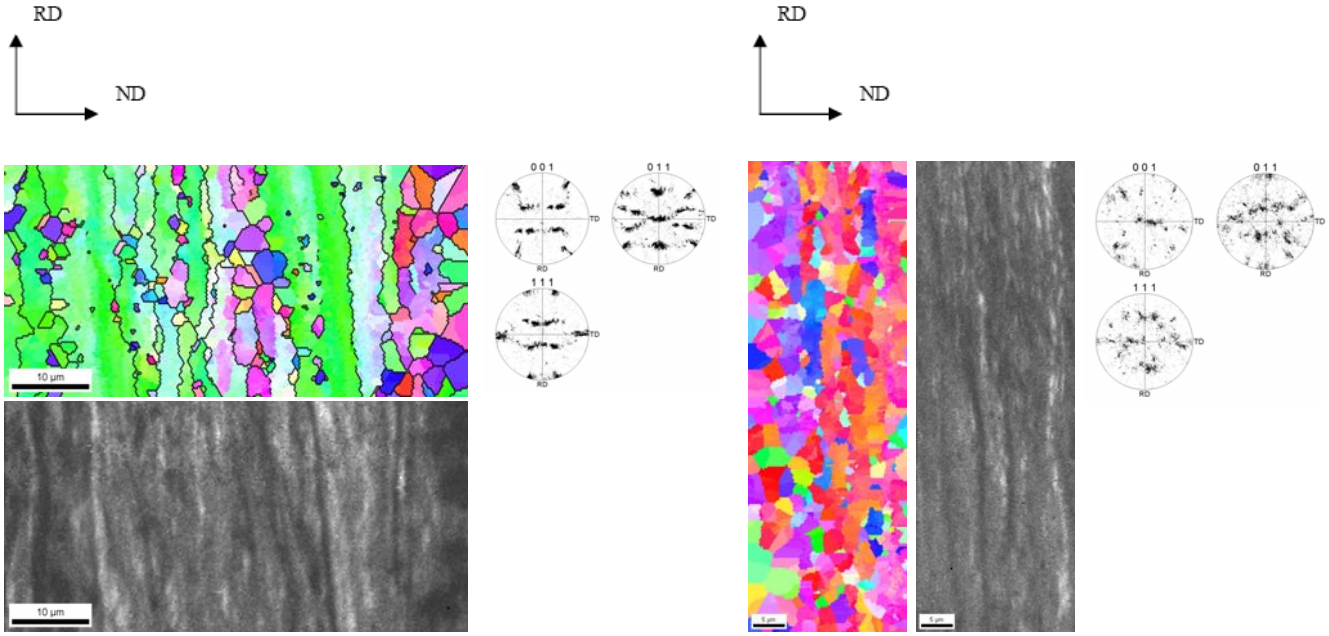

(a) (b)

Figure 10. IPF map, IQ map along the RD-ND direction and rotated pole figure (in RD-TD direction) of HB material cold rolled to 74%reduction showing (a) rolling texture in the center region and (b) shear texture closer to the surfaces in contact with the rolls.

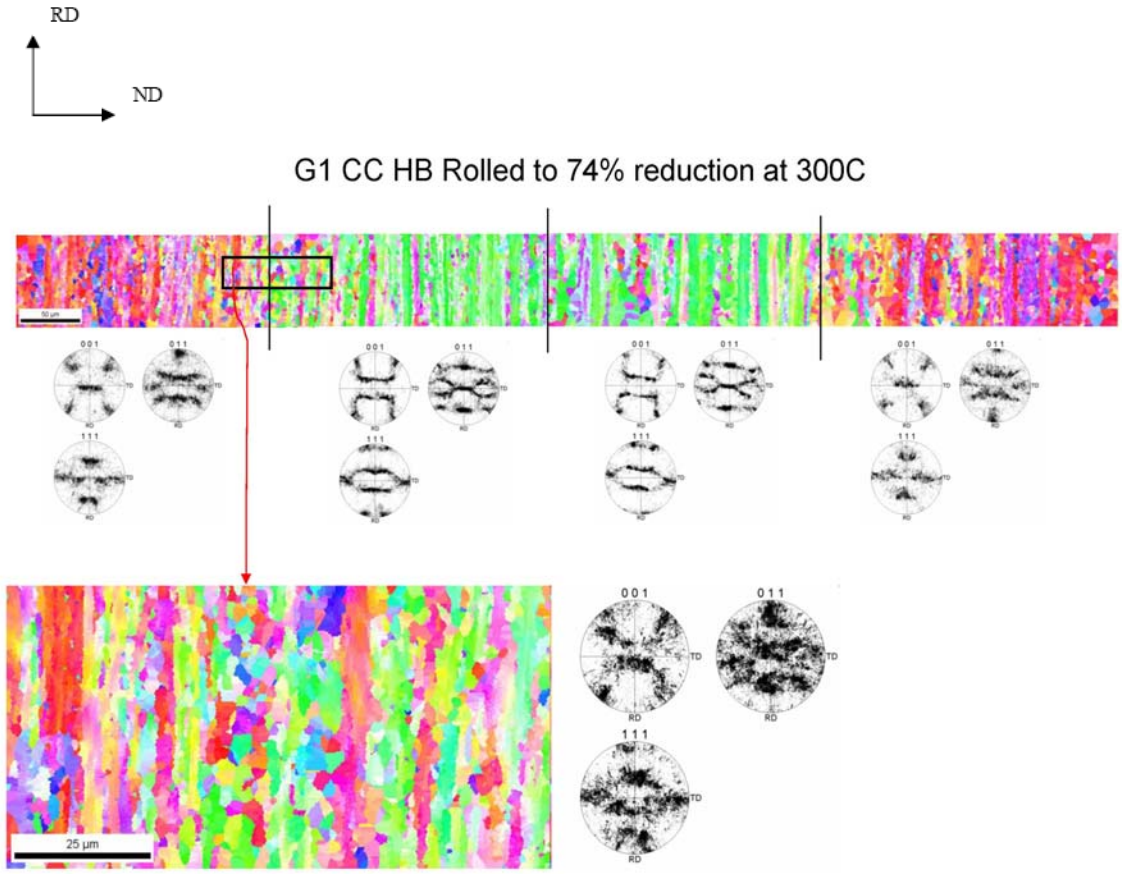

Figure 11. IPF map, IQ map along the RD-ND direction and rotated pole figure (in RD-TD direction) of HB material rolled at 300C to 74%reduction showing shear textures closer to the surfaces in contact with the rolls and rolling texture in the middle.

X-ray analysis in Figure 12 displays pole figures for the HB rolled at RT and 300°C. The results show a ND-Rotated Cube orientation in regions near the sample surface; this orientation may be expressed as {001}<110> where the notation is {plane parallel to the rolling plane}<direction parallel to the rolling direction>. The X-ray data were obtained from the surface of the rolled sheet and are consistent with the OIM data wherein a shear component predominates in the near-surface regions of the rolled sheet.

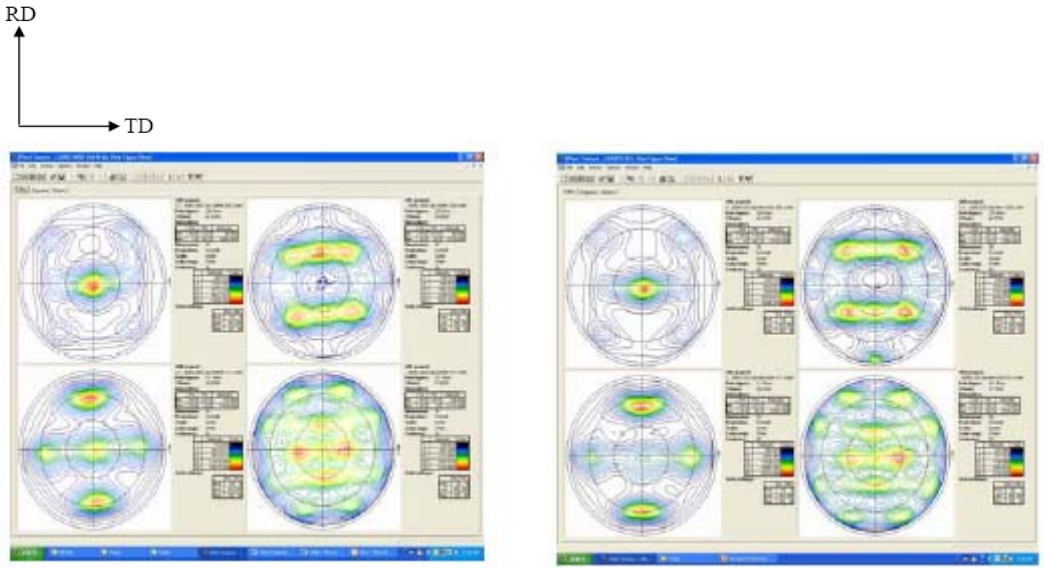

(a) (b)

Figure 12. X-ray pole figures from RD-TD plane of (a) HB rolled at RT and (b) HB rolled at 300°C showing the presence of ND rotated cube or C-component shear textures.

C. MECHANICAL PROPERTIES

Tensile tests were conducted at six strain rates between 3 x 10^{-2}/s and 3 x 10^{-4}/s. The results are shown in Figure 13. The data shows that the flow stress increases with increasing strain rate. Further analysis was conducted by determining the flow stress at a true strain of 0.1 ($\sigma_{0.1}$) from each curve and plotting this stress as a function of strain rate, as shown in Figure 14a. The slope of the resulting curve is the m-value, which is ≈ 0.33 at the lowest strain rates in this test series. Ductility data, in the form of elongation

to failure, tests are included in Figure 14b; the softer material that had been rolled at RT prior to testing exhibits consistently higher ductility over this strain rate range; nevertheless, the maximum ductility obtained was < 120 pct. The Q-parameter is defined by the relationship

$$Q = \frac{q - q^*}{q^*} \cdot 100\% \quad \text{Eq. 3}$$

where q is the reduction in area at failure and q^* is the reduction expected in the absence of flow localization. The q^* value may be determined from the elongation to failure data. Thus, the Q-parameter is a geometric parameter that indicates whether failure is controlled by cavitation or by flow localization (necking). When the Q-parameter is positive, failure is determined by flow localization; when it is negative, cavitation is contributing to failure.

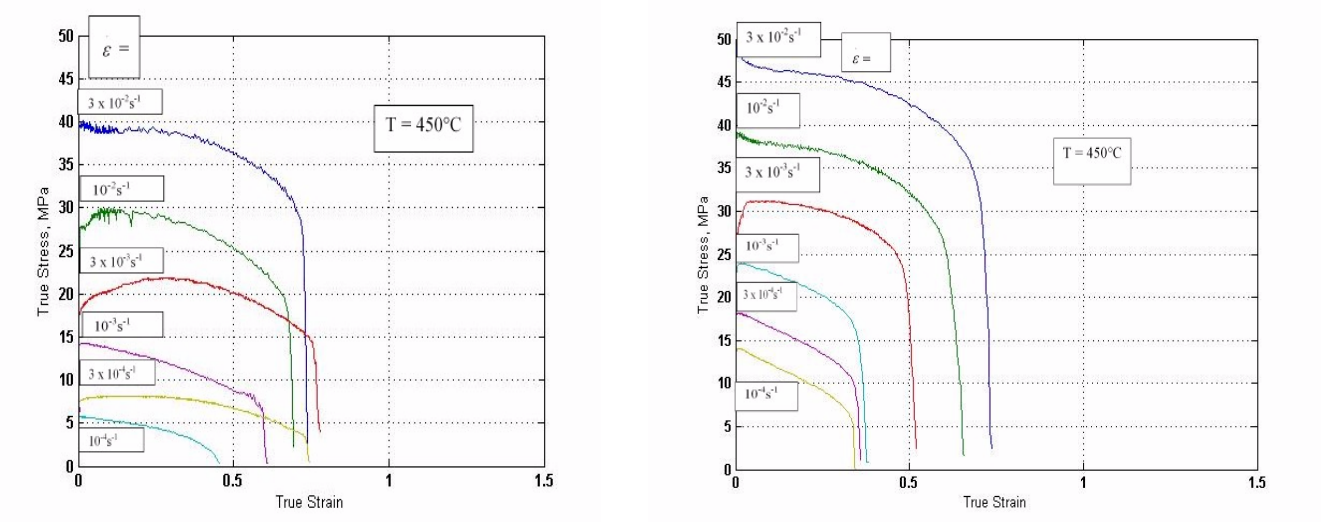

(a) (b)

Figure 13. Stress Strain curves for tensile tests done at 450°C for G1, HB material rolled to74% reduction at (a) RT and (b) 300°C.

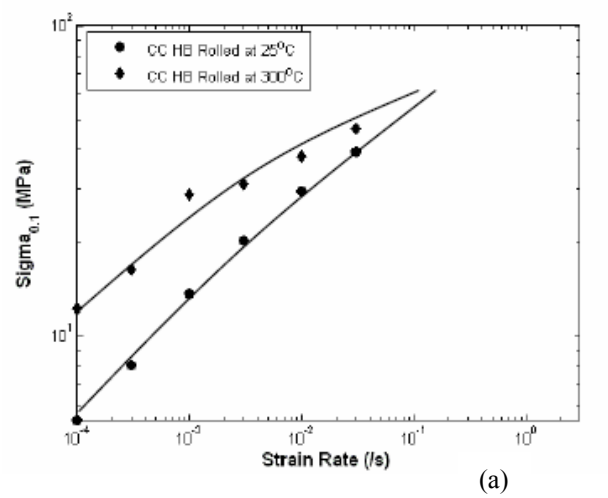

(a)

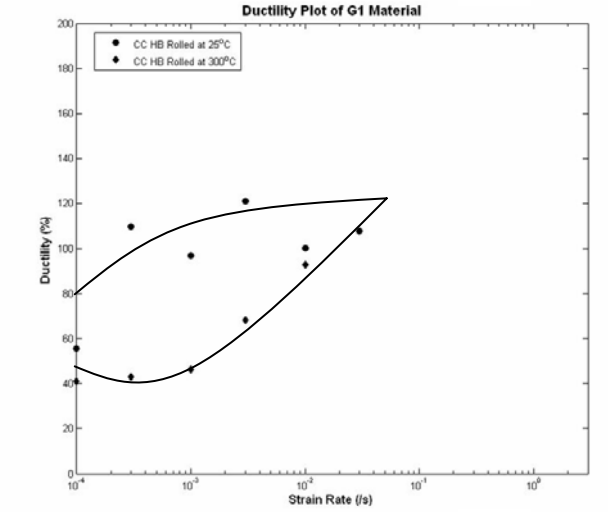

(b)

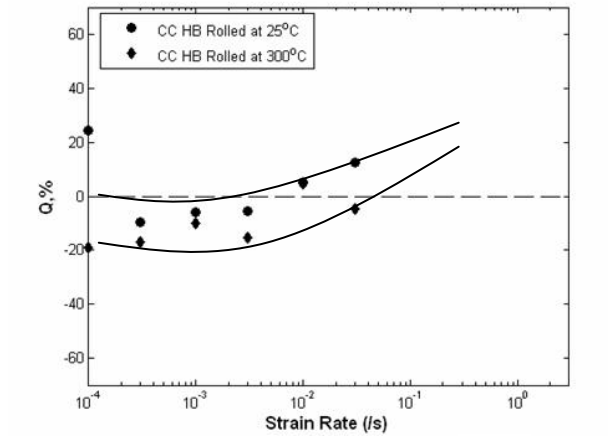

(c)

Figure 14. (a) Sigma $_{0.1}$, (b) Ductility and (c) Q% vs. S rate for HB, G1 material rolled at RT and 300°C to 74% reduction and tested at various strain rates at 450°C.

The data suggest cavitation was the controlling mechanism for the lower strain rates with flow localization only becoming the primary mechanism for the highest strain rate in the material rolled at RT. Optical fractography pictured in Figure 15 show cavitation near the point of failure.

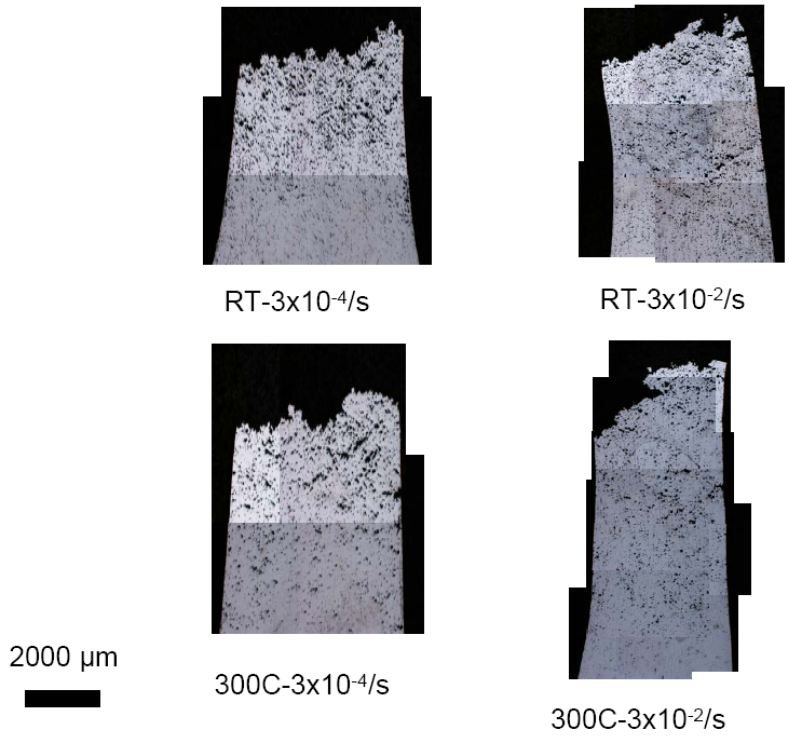

Figure 15. Optical fractographs of HB, G1 material rolled to 74% reduction at RT and 300°C for strain rates of $3x10^{-4}$/s and $3x10^{-2}$/s.

SEM fractography of the fracture surfaces is pictured in Figure 16 and show a predominance of micro void formation and coalescence.

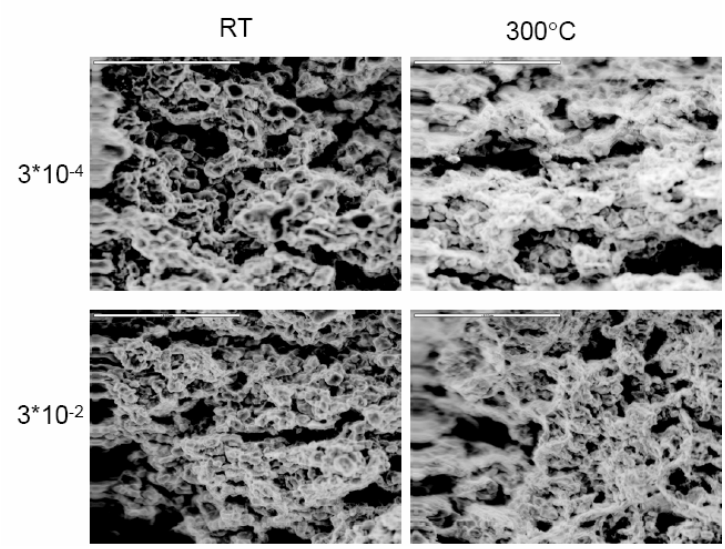

Figure 16. SEM fractographs of fractured surfaces of HB material rolled at RT and 300°C to 74% reduction and tested at 450°C at strain rates of $3x10^{-4}$/s, $3x10^{-2}$/s.

THIS PAGE INTENTIONALLY LEFT BLANK

V. DISCUSSION

OIM analysis of the CC G1 material rolled from HB to 74 % reduction revealed a Mean Linear Grain Intercept (MLI) grain size of 2.38 μm and 4.9 μm, and an area-weighted grain size of 4.33 μm and 10.46 μm for materials rolled at RT and 300°C, respectively, as shown in Figure 17. It is evident from the data that grain refinement has occurred during processing and is within the conventionally accepted superplastic regime. However, it is noted that grain refinement is notably better in the material rolled at RT, and this may be attributed to greater stored strain energy than the material rolled at 300°C. Despite the refined grain size, both RT and 300°C rolled materials show only moderate ductility compared to similar AA5083 materials processed by other methods as seen in Figure 18.

The lower ductility may be attributed to a combination of factors. The factors to be analyzed include CC to DC casting procedures and related effects on HB microstructure, effects of roll gap geometry and penetration of a shear texture, and the recrystallization mechanism during evolution of the microstructure.

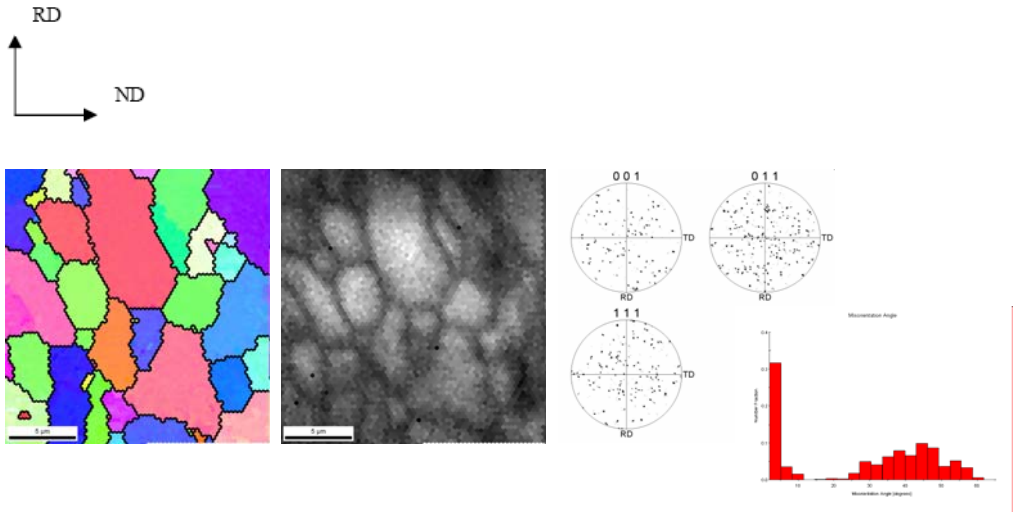

Area weighted grain size = 4.33µm
MLI = 2.38um

(a)

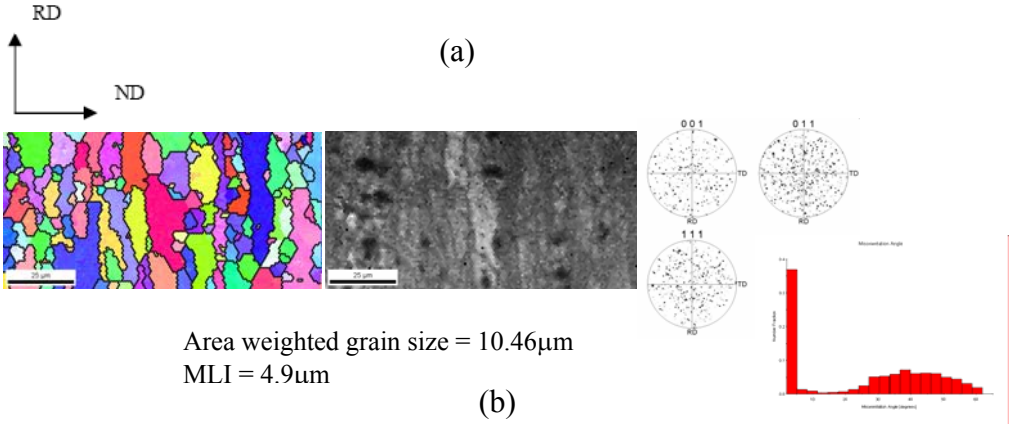

Area weighted grain size = 10.46µm
MLI = 4.9um

(b)

Figure 17. IPF map, IQ map along the RD-ND direction, rotated pole figure (in RD-TD direction) and misorientation map of (a) HB material rolled at RT and to 74% reduction and (b) HB material rolled at 300°C to 74% reduction.

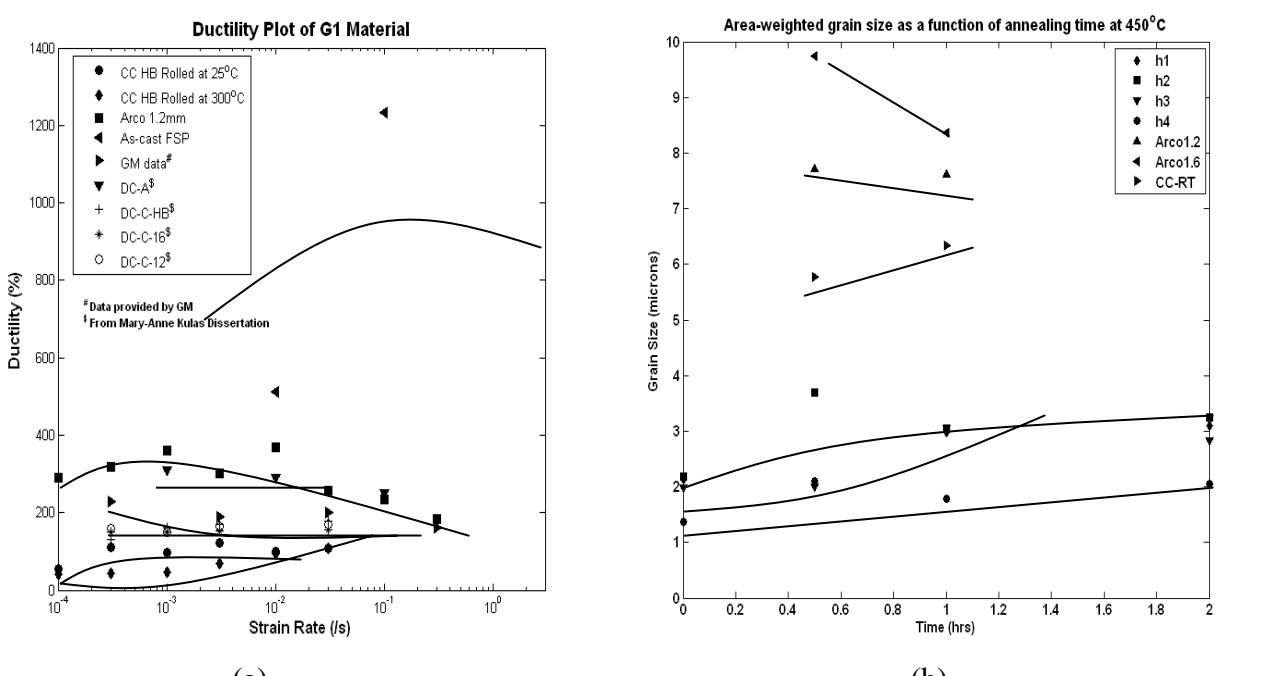

(a) (b)

Figure 18. Comparison of as-received HB, G1, CC, AA5083 material tested at 450°C at various strain rates to similar materials in (a) ductility and (b) area weighted grain size as a function of annealing time at 450° C

Differences in deformation processing lead to different textures and recrystallization behavior. DC casting involves the fabrication of cast ingots that are subsequently annealed for homogenization and then hot and warm rolled to the HB condition. This process almost completely breaks up the cast structures in the material due to the very large strains necessary to roll the material from the as-cast thickness (perhaps 300 mm) to HB thickness (e.g. 4 mm). Conversely, CC materials reach the HB condition directly from a cast state without intermediate homogenization and with significantly lower degrees of hot working. The as-cast thickness of the CC material is typically 15 mm while the HB condition is still ≈ 4 mm in thickness. As a result, CC HB material has a microstructure in which the spatial distribution of the constituent particles is not uniform. Usually, the formability of CC material is inferior to DC material [12]. It has been documented that DC HB materials show much flatter grain boundaries along the RD than the CC materials [12]. This is due to the significantly higher strain induced into the DC during high hot rolling reduction. It has also been noted that the grain size of

recrystallized CC HB is larger than recrystallized DC HB. The inhomogeneous microstructure developed in CC materials may lead to poor superplastic performance due the lack of fine, uniform and equiaxed grains required for SPF. Non-uniform particle spacing may also play a significant roll in the poor performance of the AA5083 material by allowing grain boundary migration. The excessive cavitation observed in the CC material may also indicate the effects of non-uniform particle spacing to the GBS deformation mechanism.

Finally, the roll gap geometry also may have a significant affect on through-thickness texture variation in rolled AA5083. The *l/h* ratio represents the geometry of the roll gap, where *l* represents the projected length of contact between the rolls and the specimen and *h* is the sheet thickness. *l/h* may be expressed as

$$\frac{2\sqrt{r(t_o - t_f)}}{t_o + t_f} \quad [13]$$

where *r* is the radius of the rolls = 50.8 mm, t_0 is the entering thickness and t_f is the exiting thickness. A schematic of the rolling process along with associated geometric parameters are shown in Figure 19.

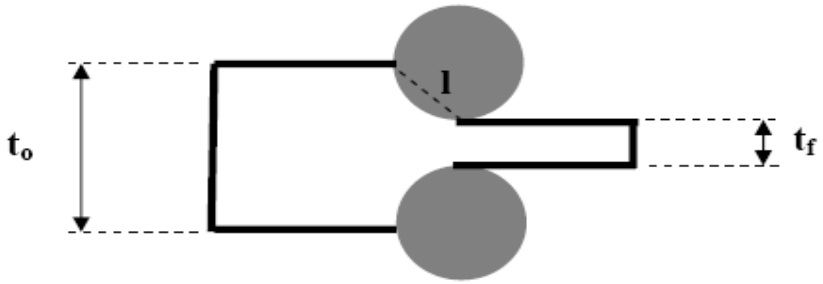

Figure 19. Schematic of rolling process along with associated geometric

At *l/h* < 0.5 shear textures are produced at and just below the surface of the sheet while at *l/h* > 5.0 a shear texture is not observed [14]. The *l/h* ratios for the rolling sequence employed here may be seen in Table 5. Although the *l/h* ratios are higher than 0.5 they

are below 5.0 and, therefore, a shear texture is expected to extend below the sheet surface. A contributing factor to the penetrating shear texture may be the friction coefficient between the rolls and the material, this may be lowered with the use of lubricants during the rolling process. The inhomogeneous texture created by the presence of shear and rolling textures in the materials may lead to inhomogeneous through-thickness variations in microstructure and hence to poor ductility.

Number of Passes	RT	300°C
1	1.84	1.36
2	2.26	2.00
3	2.77	2.26
4	2.96	2.48
5	3.02	2.77
6	3.16	3.05

Table 5. *l/h* ratios observed during rolling of HB, G1, CC, AA5083 material at RT and 300°C

GDRX is the process in which the subgrain boundaries; formed during dynamic recovery, become pinned by the particles. During deformation, these subgrain boundaries experience continuous increase in misorientation until they become typical of high-angle grain boundaries [15,16] As their misorientations increase, these sub-boundaries interact more and more strongly with the prior high-angle boundaries until new grains form. These newly formed grains may then participate in the grain boundary sliding process. This process typically involves retention of the prior deformation texture during superplastic flow. The data here, however, does not support GDRX because the strong β-fiber present in the center of the rolled material disappears and becomes random upon heating to the QPF temperature. Rather, the Particle Stimulated Nucleation (PSN) model accounts for this. The PSN is further reinforced with the observation of smaller grain sizes in the heavier strained RT rolled material. The inhomogeneous distribution of particles in the CC material may then contribute to inhomogeneous grain size, leading in turn to reduced ductility.

THIS PAGE INTENTIONALLY LEFT BLANK

VI. CONCLUSIONS

1. The as-received AA5083 hot-band, produced by CC, material displayed an elongated and banded structure correlated with a β fiber or rolling texture.
2. The cold-rolled AA5083 material displayed a smaller grain size than the material rolled at 300°C, however, both materials grain sizes were within the superplastic regime.
3. Poor to moderate ductility was obtained from the CC AA5083 HB material rolled to 74% reduction despite the refined grain size.
4. The Particle Stimulated Nucleation model seems to be the controlling factor in the microstructure formation.
5. Continuously cast AA5083 material may not have a homogenous microstructure contributing to poor SPF characteristics.
6. Roll gap geometry induces a shear texture through the material leading to an inhomogeneous microstructure and contributing to poor SPF characteristics.

THIS PAGE INTENTIONALLY LEFT BLANK

VII. FUTURE RECOMMENDATIONS

1. Examine shear texture penetration; adjust rolling schedule.
2. Examine microstructure development during CC vs. DC.
3. Conduct tensile tests at higher strain rates.
4. Adjust rolling temperature.
5. Determine a ‘window’ of processing that follows GDRX.

THIS PAGE INTENTIONALLY LEFT BLANK

LIST OF REFERENCES

[1] J. F. Boydon, Study of Cavitation and Failure Mechanisms in Superplastic 5083 Aluminum Alloy, Master's Thesis, Naval Postgraduate School, Monterey, CA, September 2003.

[2] X. D. Ding, H. M. Zbib, C. H. Hamilton, A. E. Bayoumi, *J. Eng Mat. Technol.,* v. 119, p. 26, 1997.

[3] H. Iwaski, H. Hosokawa, T. Mori, T. Tagata, K. Higashi, *Mat. Sci. Eng.,* v. A252, p. 199, 1998.

[4] T. G. Nieh, J. Wadsworth, and O. D. Sherby, *Superplasticity in Metals and Ceramics,* Cambridge University press, New York, 1997.

[5] M. T. Pérez-prado, G. González-Doncel, O. A. Ruano, and T. R. McNelley, *Acta Materialia,* v. 49, pp. 2258-2260, 2001.

[6] M. Eddahbi, T. R. McNelley, O. A. Ruano, *Metall. Trans. A,* v. 32A, p. 1093, 2001.

[7] R. W. Hertzberg, *Deformation and Fracture Mechanics of Engineering Materials*, 4th ed. New York: John Wiley & Sons, Inc., 1996.

[8] V. Randle, *Microtexture determination and Its Applications*, The Institute of Materials, 1992.

[9] B. D. Culity, *Elements of X-ray Diffraction*, Addison-Wesley Pub. Co., 1978.

[10] O. D. Sherby, Wadsworth, *Prog. Mat. Sci,* v. 33, p.169, 1989.

[11] W. Blum, Q. Zhu, R. Merkel, H. J. McQueen, *Mat. Sci. Eng.,* v. 205, pp. 23-30, 1996.

[12] Jiantao Liu, Texture and Grain Boundary Evolutions of Continuously cast and Direct Chill Cast AA5052 Aluminum Alloy During Cold Rolling, Master's Thesis, University of Kentucky, Lexington, KY, 2002.

[13] O.V. Mishin, B. Bay, and D. Juul, Jensen, *Metall. Trans. A*, v. 31A, p. 1653, 2000.

[14] W. C. Liu, J. G. Morris, Through-Thickness Texture Variation in Cold-Rolled AA5182 Aluminum Alloy with an initial {001}<110> Texture, Master's Thesis, University of Kentucky, Lexington, KY, 2004.

[15] L. M. Dougherty, J. S. Robertson, Bruemmer Vetrano, S.M., *Ma. Sci.* Forum, v. 93, pp. 357-359, 2001.

[16] L. M. Dougherty, J. S. Robertson, Vetrano, *Acta Mat.,* v. 51, p. 4367, 2003.

[17] J. W. Herrell, Analysis of the Transition in Deformation Mechanisms in Superplastic 5083 Aluminum Alloys by Orientation Imaging Microscopy, Master's Thesis, Naval Postgraduate School, Monterey, CA, September 2001.

[18] M. A. Kulas, W. P. Greene, E. M. Taleff, P. E. Krajewski, and T. R. McNelley, *Metall. Trans. A*, v. 36A, p. 1249, 2005.

[19] A. P. Zhilyaev, K. Oh-ishi, G. I. Raab, and T. R. McNelley, *Ultrafine Grained Materials IV*, Warrendale, PA, p. 113, 2006.

INITIAL DISTRIBUTION LIST

1. Defense Technical Information Center
   Ft. Belvoir, Virginia

2. Dudley Knox Library
   Naval Postgraduate School
   Monterey, California

3. Engineering and Technology Curricular Office, Code 34
   Naval Postgraduate School
   Monterey, California

4. Professor Terry R. McNelley, Code ME/Mc
   Naval Postgraduate School
   Monterey, California

5. Professor Eric Taleff
   The University of Texas at Austin
   Austin, Texas

6. Dr. Paul E. Krajewski
   General Motors Corporation
   Warren, Michigan

7. Dr. Jianqing Su
   Naval Postgraduate School
   Monterey, California

8. Dr. Srinivasan Swaminathan
   Naval Postgraduate School
   Monterey, California

9. ENS Marc T. Bland
   Naval Postgraduate School
   Monterey, California

10. LT. Matthew F. Thompson
    Naval Postgraduate School
    Monterey, California